

Measurement of charged current triple gauge boson couplings using W pairs at LEP

The OPAL Collaboration

Abstract

Triple gauge boson couplings are measured from W-pair events recorded by the OPAL detector at LEP at centre-of-mass energies of 183 – 209 GeV with a total integrated luminosity of 680 pb⁻¹. Only CP-conserving couplings are considered and SU(2)×U(1) relations are used, resulting in four independent couplings, κ_γ , g_1^z , λ_γ and g_5^z . Determining each coupling in a separate fit, assuming the other couplings to take their Standard Model values, we obtain $\kappa_\gamma=0.88_{-0.08}^{+0.09}$, $g_1^z=0.987_{-0.033}^{+0.034}$, $\lambda_\gamma=-0.060_{-0.033}^{+0.034}$ and $g_5^z=-0.04_{-0.12}^{+0.13}$, where the errors include both statistical and systematic uncertainties. Fits are also performed allowing some of the couplings to vary simultaneously. All results are consistent with the Standard Model predictions.

Submitted to the European Physical Journal C

The OPAL Collaboration

G. Abbiendi², C. Ainsley⁵, P.F. Åkesson³, G. Alexander²², J. Allison¹⁶, P. Amaral⁹,
G. Anagnostou¹, K.J. Anderson⁹, S. Arcelli², S. Asai²³, D. Axen²⁷, G. Azuelos^{18,a}, I. Bailey²⁶,
E. Barberio^{8,p}, R.J. Barlow¹⁶, R.J. Batley⁵, P. Bechtel²⁵, T. Behnke²⁵, K.W. Bell²⁰, P.J. Bell¹,
G. Bella²², A. Bellerive⁶, G. Benelli⁴, S. Bethke³², O. Biebel³¹, O. Boeriu¹⁰, P. Bock¹¹,
M. Boutemour³¹, S. Braibant⁸, L. Brigliadori², R.M. Brown²⁰, K. Buesser²⁵, H.J. Burckhart⁸,
S. Campana⁴, R.K. Carnegie⁶, B. Caron²⁸, A.A. Carter¹³, J.R. Carter⁵, C.Y. Chang¹⁷,
D.G. Charlton¹, A. Csilling²⁹, M. Cuffiani², S. Dado²¹, A. De Roeck⁸, E.A. De Wolf^{8,s},
K. Desch²⁵, B. Dienes³⁰, M. Donkers⁶, J. Dubbert³¹, E. Duchovni²⁴, G. Duckeck³¹,
I.P. Duerdoth¹⁶, E. Etzion²², F. Fabbri², L. Feld¹⁰, P. Ferrari⁸, F. Fiedler³¹, I. Fleck¹⁰, M. Ford⁵,
A. Frey⁸, A. Fürtjes⁸, P. Gagnon¹², J.W. Gary⁴, G. Gaycken²⁵, C. Geich-Gimbel³,
G. Giacomelli², P. Giacomelli², M. Giunta⁴, J. Goldberg²¹, E. Gross²⁴, J. Grunhaus²²,
M. Gruwé⁸, P.O. Günther³, A. Gupta⁹, C. Hajdu²⁹, M. Hamann²⁵, G.G. Hanson⁴, K. Harder²⁵,
A. Harel²¹, M. Harin-Dirac⁴, M. Hauschild⁸, C.M. Hawkes¹, R. Hawkings⁸, R.J. Hemingway⁶,
C. Hensel²⁵, G. Herten¹⁰, R.D. Heuer²⁵, J.C. Hill⁵, K. Hoffman⁹, D. Horváth^{29,c},
P. Igo-Kemenes¹¹, K. Ishii²³, H. Jeremie¹⁸, P. Jovanovic¹, T.R. Junk⁶, N. Kanaya²⁶,
J. Kanzaki^{23,u}, G. Karapetian¹⁸, D. Karlen²⁶, K. Kawagoe²³, T. Kawamoto²³, R.K. Keeler²⁶,
R.G. Kellogg¹⁷, B.W. Kennedy²⁰, D.H. Kim¹⁹, K. Klein^{11,t}, A. Klier²⁴, S. Kluth³²,
T. Kobayashi²³, M. Kobel³, S. Komamiya²³, L. Kormos²⁶, T. Krämer²⁵, P. Krieger^{6,l}, J. von
Krogh¹¹, K. Kruger⁸, T. Kuhl²⁵, M. Kupper²⁴, G.D. Lafferty¹⁶, H. Landsman²¹, D. Lanske¹⁴,
J.G. Layter⁴, A. Leins³¹, D. Lellouch²⁴, J. Letts^o, L. Levinson²⁴, J. Lillich¹⁰, A.W. Lloyd¹,
S.L. Lloyd¹³, F.K. Loebinger¹⁶, J. Lu^{27,w}, J. Ludwig¹⁰, A. Macchiolo^{18,x}, A. Macpherson^{28,i},
W. Mader³, S. Marcellini², A.J. Martin¹³, G. Masetti², T. Mashimo²³, P. Mättig^m,
W.J. McDonald²⁸, J. McKenna²⁷, T.J. McMahon¹, R.A. McPherson²⁶, F. Meijers⁸,
W. Menges²⁵, F.S. Merritt⁹, H. Mes^{6,a}, A. Michelini², S. Mihara²³, G. Mikenberg²⁴,
D.J. Miller¹⁵, S. Moed²¹, W. Mohr¹⁰, T. Mori²³, A. Mutter¹⁰, K. Nagai¹³, I. Nakamura^{23,v},
H. Nanjo²³, H.A. Neal³³, R. Nisius³², S.W. O’Neale¹, A. Oh⁸, A. Okpara¹¹, M.J. Oreglia⁹,
S. Orito^{23,*}, C. Pahl³², G. Pásztor^{4,g}, J.R. Pater¹⁶, G.N. Patrick²⁰, J.E. Pilcher⁹, J. Pinfold²⁸,
D.E. Plane⁸, B. Poli², J. Polok⁸, O. Pooth¹⁴, M. Przybycien^{8,n}, A. Quadt³, K. Rabbertz^{8,r},
C. Rembser⁸, P. Renkel²⁴, J.M. Roney²⁶, S. Rosati³, K. Roscoe¹⁶, Y. Rozen²¹, K. Runge¹⁰,
K. Sachs⁶, T. Saeki²³, E.K.G. Sarkisyan^{8,j}, C. Sbarra^{26,y}, A.D. Schaile³¹, O. Schaile³¹,
P. Scharff-Hansen⁸, J. Schieck³², T. Schörner-Sadenius⁸, M. Schröder⁸, M. Schumacher³,
C. Schwick⁸, W.G. Scott²⁰, R. Seuster^{14,f}, T.G. Shears^{8,h}, B.C. Shen⁴, P. Sherwood¹⁵, G. Sirolì²,
A. Skuja¹⁷, A.M. Smith⁸, R. Sobie²⁶, S. Söldner-Rembold^{16,d}, F. Spano⁹, A. Stahl³,
K. Stephens¹⁶, D. Strom¹⁹, R. Ströhmer³¹, S. Tarem²¹, M. Tasevsky⁸, R.J. Taylor¹⁵,
R. Teuscher⁹, M.A. Thomson⁵, E. Torrence¹⁹, D. Toya²³, P. Tran⁴, I. Trigger⁸, Z. Trócsányi^{30,e},
E. Tsur²², M.F. Turner-Watson¹, I. Ueda²³, B. Ujvári^{30,e}, C.F. Vollmer³¹, P. Vannerem¹⁰,
R. Vértési³⁰, M. Verzocchi¹⁷, H. Voss^{8,q}, J. Vossebeld^{8,h}, D. Waller⁶, C.P. Ward⁵, D.R. Ward⁵,
P.M. Watkins¹, A.T. Watson¹, N.K. Watson¹, P.S. Wells⁸, T. Wengler⁸, N. Wermes³,
D. Wetterling¹¹, G.W. Wilson^{16,k}, J.A. Wilson¹, G. Wolf²⁴, T.R. Wyatt¹⁶, S. Yamashita²³,
D. Zer-Zion⁴, L. Zivkovic²⁴

¹School of Physics and Astronomy, University of Birmingham, Birmingham B15 2TT, UK

²Dipartimento di Fisica dell’ Università di Bologna and INFN, I-40126 Bologna, Italy

- ³Physikalisches Institut, Universität Bonn, D-53115 Bonn, Germany
- ⁴Department of Physics, University of California, Riverside CA 92521, USA
- ⁵Cavendish Laboratory, Cambridge CB3 0HE, UK
- ⁶Ottawa-Carleton Institute for Physics, Department of Physics, Carleton University, Ottawa, Ontario K1S 5B6, Canada
- ⁸CERN, European Organisation for Nuclear Research, CH-1211 Geneva 23, Switzerland
- ⁹Enrico Fermi Institute and Department of Physics, University of Chicago, Chicago IL 60637, USA
- ¹⁰Fakultät für Physik, Albert-Ludwigs-Universität Freiburg, D-79104 Freiburg, Germany
- ¹¹Physikalisches Institut, Universität Heidelberg, D-69120 Heidelberg, Germany
- ¹²Indiana University, Department of Physics, Bloomington IN 47405, USA
- ¹³Queen Mary and Westfield College, University of London, London E1 4NS, UK
- ¹⁴Technische Hochschule Aachen, III Physikalisches Institut, Sommerfeldstrasse 26-28, D-52056 Aachen, Germany
- ¹⁵University College London, London WC1E 6BT, UK
- ¹⁶Department of Physics, Schuster Laboratory, The University, Manchester M13 9PL, UK
- ¹⁷Department of Physics, University of Maryland, College Park, MD 20742, USA
- ¹⁸Laboratoire de Physique Nucléaire, Université de Montréal, Montréal, Québec H3C 3J7, Canada
- ¹⁹University of Oregon, Department of Physics, Eugene OR 97403, USA
- ²⁰CLRC Rutherford Appleton Laboratory, Chilton, Didcot, Oxfordshire OX11 0QX, UK
- ²¹Department of Physics, Technion-Israel Institute of Technology, Haifa 32000, Israel
- ²²Department of Physics and Astronomy, Tel Aviv University, Tel Aviv 69978, Israel
- ²³International Centre for Elementary Particle Physics and Department of Physics, University of Tokyo, Tokyo 113-0033, and Kobe University, Kobe 657-8501, Japan
- ²⁴Particle Physics Department, Weizmann Institute of Science, Rehovot 76100, Israel
- ²⁵Universität Hamburg/DESY, Institut für Experimentalphysik, Notkestrasse 85, D-22607 Hamburg, Germany
- ²⁶University of Victoria, Department of Physics, P O Box 3055, Victoria BC V8W 3P6, Canada
- ²⁷University of British Columbia, Department of Physics, Vancouver BC V6T 1Z1, Canada
- ²⁸University of Alberta, Department of Physics, Edmonton AB T6G 2J1, Canada
- ²⁹Research Institute for Particle and Nuclear Physics, H-1525 Budapest, P O Box 49, Hungary
- ³⁰Institute of Nuclear Research, H-4001 Debrecen, P O Box 51, Hungary
- ³¹Ludwig-Maximilians-Universität München, Sektion Physik, Am Coulombwall 1, D-85748 Garching, Germany
- ³²Max-Planck-Institute für Physik, Föhringer Ring 6, D-80805 München, Germany
- ³³Yale University, Department of Physics, New Haven, CT 06520, USA

^a and at TRIUMF, Vancouver, Canada V6T 2A3

^c and Institute of Nuclear Research, Debrecen, Hungary

^d and Heisenberg Fellow

^e and Department of Experimental Physics, Lajos Kossuth University, Debrecen, Hungary

^f and MPI München

^g and Research Institute for Particle and Nuclear Physics, Budapest, Hungary

^h now at University of Liverpool, Dept of Physics, Liverpool L69 3BX, U.K.

ⁱ and CERN, EP Div, 1211 Geneva 23

^j and Manchester University

- k* now at University of Kansas, Dept of Physics and Astronomy, Lawrence, KS 66045, U.S.A.
- l* now at University of Toronto, Dept of Physics, Toronto, Canada
- m* current address Bergische Universität, Wuppertal, Germany
- n* now at University of Mining and Metallurgy, Cracow, Poland
- o* now at University of California, San Diego, U.S.A.
- p* now at Physics Dept Southern Methodist University, Dallas, TX 75275, U.S.A.
- q* now at IPHE Université de Lausanne, CH-1015 Lausanne, Switzerland
- r* now at IEKP Universität Karlsruhe, Germany
- s* now at Universitaire Instelling Antwerpen, Physics Department, B-2610 Antwerpen, Belgium
- t* now at RWTH Aachen, Germany
- u* and High Energy Accelerator Research Organisation (KEK), Tsukuba, Ibaraki, Japan
- v* now at University of Pennsylvania, Philadelphia, Pennsylvania, USA
- w* now at TRIUMF, Vancouver, Canada
- x* now at University of Florence, Florence, Italy.
- y* now at IASF-CNR Sezione di Bologna, 40129 Bologna, Italy.
- * Deceased

1 Introduction

The triple gauge boson vertices, $WW\gamma$ and WWZ , are expected in the Standard Model due to its non-Abelian nature. The Standard Model predicts exact values of the associated parameters, the triple gauge boson couplings (TGCs). Any significant deviation of the measured values from this prediction would be a signature of new physics beyond the Standard Model. Several measurements of these couplings have already been performed at LEP using W-pair [1–5], single W [6] and single photon [7] production. Limits on TGCs also exist from studies of di-boson production at the Tevatron [8]. This paper reports results on TGCs using W-pair events from the full OPAL LEP2 data sample.

Assuming a general Lorentz-invariant Lagrangian which satisfies electromagnetic gauge invariance, charge conjugation (C) and parity (P) invariance, five independent TGC parameters are expected to describe the $WW\gamma$ and WWZ vertices. These can be taken as g_1^z , κ_z , κ_γ , λ_z and λ_γ [9–12]. In the Standard Model $g_1^z = \kappa_z = \kappa_\gamma = 1$ and $\lambda_z = \lambda_\gamma = 0$. When the restriction on C and P invariance is dropped, but their product, CP, is required to be invariant, a sixth coupling, g_5^z [9–12], which violates both C and P, is added. This coupling vanishes in the Standard Model. Couplings which violate CP [13] are not considered in this analysis.

Precision measurements on the Z^0 resonance and lower energy data motivate the following $SU(2) \times U(1)$ relations between the five C and P conserving couplings [9, 11],

$$\begin{aligned}\Delta\kappa_z &= -\Delta\kappa_\gamma \tan^2 \theta_w + \Delta g_1^z, \\ \lambda_z &= \lambda_\gamma.\end{aligned}$$

Here Δ indicates a deviation of the respective quantity from its Standard Model value and θ_w is the weak mixing angle at tree level, defined by $\cos \theta_w = M_W/M_Z$. These two relations leave three independent C and P conserving couplings, $\Delta\kappa_\gamma$, Δg_1^z and $\lambda(=\lambda_\gamma=\lambda_z)$, plus the C and P violating coupling g_5^z . These couplings are not significantly restricted [14, 15] by measurements from data collected at the Z^0 pole at LEP and SLC.

While the single W and single photon processes can also be used to measure TGCs, W-pair production is by far the most sensitive process for this measurement. Its sensitivity comes from the triple gauge boson vertex connecting the intermediate s -channel Z^0/γ to the outgoing W-bosons. The TGC contribution depends on the helicity states of the outgoing W bosons, determining the angular distributions of the W bosons and of their decay products. The total W-pair cross-section is also affected by the TGCs, but for centre-of-mass energies well above the threshold for W-pair production and for small values of anomalous couplings its sensitivity, compared with the angular distributions, is much lower. Very often, however, the angular distribution analysis yields two ambiguous solutions for the TGCs, one being quite far away from the Standard Model values [16], and the information from the total cross-section can help in resolving this ambiguity.

The production and decay of W-pair events can be characterized by five angular variables. These are the W^- production polar angle¹, θ_W , the polar and azimuthal angles, θ^* and ϕ^* ,

¹The OPAL right-handed coordinate system is defined such that the origin is at the centre of the detector, the z -axis is parallel to, and has positive sense along, the e^- beam direction, θ is the polar angle with respect to z and ϕ is the azimuthal angle around z with respect to the x -axis, which points to the centre of the LEP ring.

of the decay fermion from the W^- in the W^- rest frame², and the corresponding polar and azimuthal angles of the decay anti-fermion from the W^+ . The experimental accessibility of these angles depends on the final state produced when the W bosons decay.

All W -pair final states are used in this study, namely the leptonic, $\ell\bar{\nu}_\ell\bar{\ell}'\nu_{\ell'}$, the semileptonic, $q\bar{q}\ell\bar{\nu}_\ell$, and the hadronic, $q\bar{q}q\bar{q}$ final states, with branching fractions of 10.5%, 43.9% and 45.6% respectively in the Standard Model.

The next section discusses the OPAL data and Monte Carlo samples. The following three sections then present the first part of this study using the W -pair angular distributions. For this purpose, the kinematic observables of each event are reconstructed as described in Section 3 and then used in Section 4 to construct optimal observables and analyse them in terms of the TGCs. The study of systematic errors for this part of the analysis is summarised in Section 5. Section 6 describes the second part of this analysis, where the total W -pair event rate is used to extract additional information on the TGCs. The TGC results are presented in Section 7 and summarised in the last section.

2 Data and Monte Carlo samples

The OPAL detector is described in detail elsewhere [17]. The data were collected during 1997-2000 around eight different centre-of-mass energies. The integrated luminosity at each energy is evaluated using small angle Bhabha scattering events observed in the silicon tungsten forward calorimeter. The luminosity-weighted average values of the centre-of-mass energies and the corresponding luminosities are listed in Table 1.

The main Monte Carlo generator used to simulate the W -pair signal is Kandy, which is a combination of KORALW1.51 [18] and YFSWW3 [19] running concurrently. These programs generate all four-fermion final states using the full set of electroweak diagrams including the W^+W^- production diagrams (class³ CC03) and other four-fermion graphs, such as $e^+e^- \rightarrow W\bar{\nu}_e$, $e^+e^- \rightarrow Z^0e^+e^-$ and $e^+e^- \rightarrow Z^0Z^0$. All diagrams are corrected for initial and final state radiation, while a more complete correction of $\mathcal{O}(\alpha)$ radiative effects is applied to the CC03 diagrams. For each centre-of-mass energy, 500,000 events have been generated using these Monte Carlo programs, and these events are used as our reference samples for the TGC analysis. The TGC dependence is obtained by reweighting these samples using the four-fermion matrix element calculation taken from the EXCALIBUR [20] Monte Carlo program. This program has also been used to generate samples with anomalous TGCs which are used to cross-check our TGC extraction method. Although EXCALIBUR includes less complete $\mathcal{O}(\alpha)$ radiative effects, it can still be used for small anomalous TGC values, where the effect of the missing $\mathcal{O}(\alpha)$ corrections on the anomalous TGC contribution can be neglected.

Background sources to the W -pair signal are four-fermion final states, such as $q\bar{q}\ell\bar{\ell}$, which are

²The axes of the right-handed coordinate system in the W rest-frame are defined such that the z -axis is along the parent W flight direction in the overall centre-of-mass system, and the y -axis is in the direction $\vec{e}^+ \times \vec{W}$ where \vec{e}^+ is the electron beam direction and \vec{W} is the parent W flight direction.

³In this paper, the three lowest order W -pair production diagrams, *i.e.* t -channel ν_e exchange and s -channel Z^0/γ exchange, are referred to as ‘‘CC03’’, following the notation of [9].

produced only by diagrams that do not involve the triple gauge boson vertex, two-fermion final states and two-photon processes. The four-fermion background is generated using KORALW1.42 [21] and `grc4f` [22]. As an alternative for systematic studies we replace KORALW1.42 by EXCALIBUR. Two-fermion final states are generated using KK2F [23]. For systematic studies, KORALZ [24], for $e^+e^- \rightarrow \mu^+\mu^-$, $e^+e^- \rightarrow \tau^+\tau^-$ and $e^+e^- \rightarrow \nu\bar{\nu}$, and BHWIDE [25], for $e^+e^- \rightarrow e^+e^-$, are also used. Background to the semileptonic final state from single-tag two-photon processes, where the outgoing electron or positron is detected, is evaluated using HERWIG [26], and F2GEN [27] is used as an alternative for systematic studies. Background from leptonic final states from untagged two-photon processes, where both outgoing electron and positron escape undetected into the beam pipe, is calculated using the Vermaseren [28] and BDK [29] generators.

To estimate the fragmentation and hadronisation systematics, Monte Carlo samples of W^+W^- events were produced by the KORALW1.42 generator, with the fragmentation and hadronisation stages generated separately by either PYTHIA5.7 [30], HERWIG6.2 [26] or ARIADNE4.08 [31]. These hadronic simulation generators have been tuned to Z^0 hadronic decays [32]. Similarly, for the $Z^0/\gamma \rightarrow q\bar{q}$ background, the same hadronic simulation programs have been used to fragment and hadronise events produced by the KK2F generator.

All Monte Carlo samples mentioned above were processed by the full OPAL simulation program [33] and then reconstructed in the same way as the data.

3 W-pair event selection and reconstruction

W-pair events are selected with the same procedure used in the W-pair cross-section measurement as described in references [3, 34]. There are three independent selections corresponding to the three final states. Each candidate is then reconstructed in order to obtain the maximum possible information on the W production and decay angles, which are needed to extract the couplings. Events which cannot be well reconstructed are rejected from the sample, as will be described below. The numbers of candidates left at the different centre-of-mass energies for the three final states are listed, along with the expected values, in Table 1.

Three kinematic fits with different sets of requirements are used in the event reconstruction:

- A. Require conservation of energy and momentum, neglecting Initial State Radiation (ISR).
- B. Additionally constrain the reconstructed masses of the two W-bosons to be equal.
- C. Additionally constrain each reconstructed W mass to the average measured value from the Tevatron⁴, $M_W = 80.456 \text{ GeV}/c^2$ [35].

For $q\bar{q}q\bar{q}$ events, where all four final state fermions are measurable, fits A, B and C have 4, 5 and 6 constraints respectively. For $q\bar{q}e\bar{\nu}_e$ and $q\bar{q}\mu\bar{\nu}_\mu$ events the number of constraints is reduced

⁴The LEP results for the W mass are not used for the TGC measurement, since they have been obtained under the assumption that W pairs are produced according to the Standard Model, whereas W production at the Tevatron does not involve the triple gauge boson vertex.

\sqrt{s} (GeV)	$\int \mathcal{L} dt$ (pb ⁻¹)	q $\bar{q}\ell\bar{\nu}_\ell$ events		q $\bar{q}q\bar{q}$ events		$\ell\bar{\nu}_\ell\bar{\ell}\nu_\ell$ events	
		Observed	Expected	Observed	Expected	Observed	Expected
182.7	57.4	328	331.1	408	418.9	32	37.4
188.6	183.0	1090	1123.5	1437	1388.3	130	124.3
191.6	29.3	168	182.8	223	222.8	19	19.9
195.5	76.4	513	478.9	637	594.3	55	52.5
199.5	76.6	451	479.7	557	585.0	52	52.1
201.6	37.7	230	236.3	296	286.1	32	25.3
204.9	81.6	475	512.4	578	606.5	47	53.2
206.6	136.5	899	854.0	1051	1012.3	92	90.0
all	678.5	4154	4198.7	5187	5114.2	459	454.7

Table 1: Observed and expected numbers of data candidates selected for the angular distribution analysis after all cuts in the different final states and for different centre-of-mass energies.

by 3 due to the invisible neutrino. For q $\bar{q}\tau\bar{\nu}_\tau$ events there is at least one additional unobserved neutrino from the τ decay, resulting in a loss of one constraint. The momentum sum of the track(s) assigned to the τ can still be used as an approximation of the τ flight direction, relying on its high boost, but the τ energy is left unknown. Finally for $\ell\bar{\nu}_\ell\bar{\ell}\nu_\ell$ events, where none of the leptons is a τ , there are two invisible neutrinos. Hence, six constraints are lost and only requirement C is applied.

In the following we discuss the reconstruction of each final state separately.

3.1 Reconstruction of q $\bar{q}\ell\bar{\nu}_\ell$ final states

Starting from the sample used for the W-pair cross-section measurement, we select candidate q $\bar{q}e\bar{\nu}_e$ and q $\bar{q}\mu\bar{\nu}_\mu$ events with a reconstructed lepton track. The track charge is needed to reconstruct the W^- polar angle. For the q $\bar{q}\tau\bar{\nu}_\tau$ events, either one track or a narrow jet consisting of three tracks is assigned as the τ decay product.

The OPAL tracking detectors are used to reconstruct the muon momentum and the electron direction, whereas the electromagnetic calorimeters are used to give a more accurate measurement of the electron energy. As explained above, the direction of τ candidates is given directly by the τ decay products, whilst the energy of the τ is estimated using a kinematic fit.

The remaining tracks and calorimeter clusters in the event are grouped into two jets using the Durham k_\perp algorithm [36]. The total energy and momentum of each of the jets are calculated using the charged track momenta and calorimeter energies and correcting for double counting employing the method described in [37].

The different kinematic fits described above are used to improve the resolution in the five kinematic variables used for the TGC analysis. This resolution is correlated with the kinematic fit probabilities which indicate the event reconstruction quality. Therefore we use the results of the kinematic fits to classify the events into nine quality classes which are used later in the TGC analysis. The exact definitions of these classes and the fraction of accepted events in each class

Class	Final state	% of events	Requirements on fits A, B, C	Kinem. variables taken from
a)	$q\bar{q}e\bar{\nu}_e, q\bar{q}\mu\bar{\nu}_\mu$	30.4	$P_C \geq 0.20$	fit C
b)	$q\bar{q}e\bar{\nu}_e, q\bar{q}\mu\bar{\nu}_\mu$	10.1	$0.05 \leq P_C < 0.20$	fit C
c)	$q\bar{q}e\bar{\nu}_e, q\bar{q}\mu\bar{\nu}_\mu$	6.9	$0.01 \leq P_C < 0.05$	fit C
d)	$q\bar{q}e\bar{\nu}_e, q\bar{q}\mu\bar{\nu}_\mu$	4.7	$0.001 \leq P_C < 0.01$	fit A
e)	$q\bar{q}e\bar{\nu}_e, q\bar{q}\mu\bar{\nu}_\mu$	10.0	$P_C < 0.001$	fit A
f)	$q\bar{q}e\bar{\nu}_e, q\bar{q}\mu\bar{\nu}_\mu$	8.3	C failed, $P_A \geq 0.001$	fit A
g)	$q\bar{q}e\bar{\nu}_e, q\bar{q}\mu\bar{\nu}_\mu$	1.2	C failed, A failed or $P_A < 0.001$	directly measured
h)	$q\bar{q}\tau\bar{\nu}_\tau$	21.7	$P_B \geq 0.20$	fit B
i)	$q\bar{q}\tau\bar{\nu}_\tau$	6.8	$0.025 \leq P_B < 0.20$	fit A

Table 2: Definition of the nine quality classes of $q\bar{q}\ell\bar{\nu}_\ell$ events. P_A , P_B and P_C are the probabilities of kinematic fits A, B and C.

are listed in Table 2. The event population in each class is well modelled by the Monte Carlo. To optimize the resolution in the kinematic variables used in the TGC analysis they are taken, according to the quality class, either from the directly measured values or from one of the three kinematic fits, as detailed in Table 2. The $q\bar{q}\tau\bar{\nu}_\tau$ events which fail kinematic fit B or pass it with fit probability below 0.025 are rejected. This cut suppresses those $q\bar{q}\tau\bar{\nu}_\tau$ events which are correctly identified as belonging to this decay channel but where the τ decay products are not identified correctly, leading to an incorrect estimate of the τ flight direction or its charge. The fraction of such events in the $q\bar{q}\tau\bar{\nu}_\tau$ sample is thus reduced from 18% to 12%.

Finally, the kinematic variables are used to calculate the optimal observables (see Section 4) which are used to extract the TGCs. Those events (typically 1% of the sample) with optimal observable values in the far tails of their distributions are interpreted as being badly measured and discarded.

Performing the complete analysis on Monte Carlo samples generated with different anomalous couplings shows that our event selection does not introduce any bias on the TGC results.

The purities of the final samples are about 96%, 98% and 91% for the $q\bar{q}e\bar{\nu}_e$, $q\bar{q}\mu\bar{\nu}_\mu$ and $q\bar{q}\tau\bar{\nu}_\tau$ final states respectively. The background consists mainly of TGC-independent four-fermion final states and $Z^0/\gamma \rightarrow q\bar{q}$ events. Cross migration between the $q\bar{q}\tau\bar{\nu}_\tau$ and each of the $q\bar{q}e\bar{\nu}_e$ and $q\bar{q}\mu\bar{\nu}_\mu$ decay channels is at the level of 4-5% and is considered as signal.

In the reconstruction of the $q\bar{q}\ell\bar{\nu}_\ell$ events we obtain $\cos\theta_W$ by summing the kinematically fitted four-momenta of the two jets. The decay angles of the leptonically decaying W are obtained from the charged lepton four-momentum, after boosting back to the parent W rest frame. For the hadronically decaying W it is not possible to distinguish between the jets of the quark and anti-quark. This ambiguity is taken into account in the analysis described below.

In Figure 1 we show the distributions of the five angles corresponding to the $q\bar{q}\ell\bar{\nu}_\ell$ data sample and the expected distributions for $\lambda = \pm 0.5$ and 0. These expected distributions are obtained from Standard Model Monte Carlo samples. To produce the $\lambda = \pm 0.5$ distributions the events have been appropriately reweighted using the EXCALIBUR matrix element calculation. All Monte Carlo distributions are normalised to the number of events observed in the data. The

OPAL

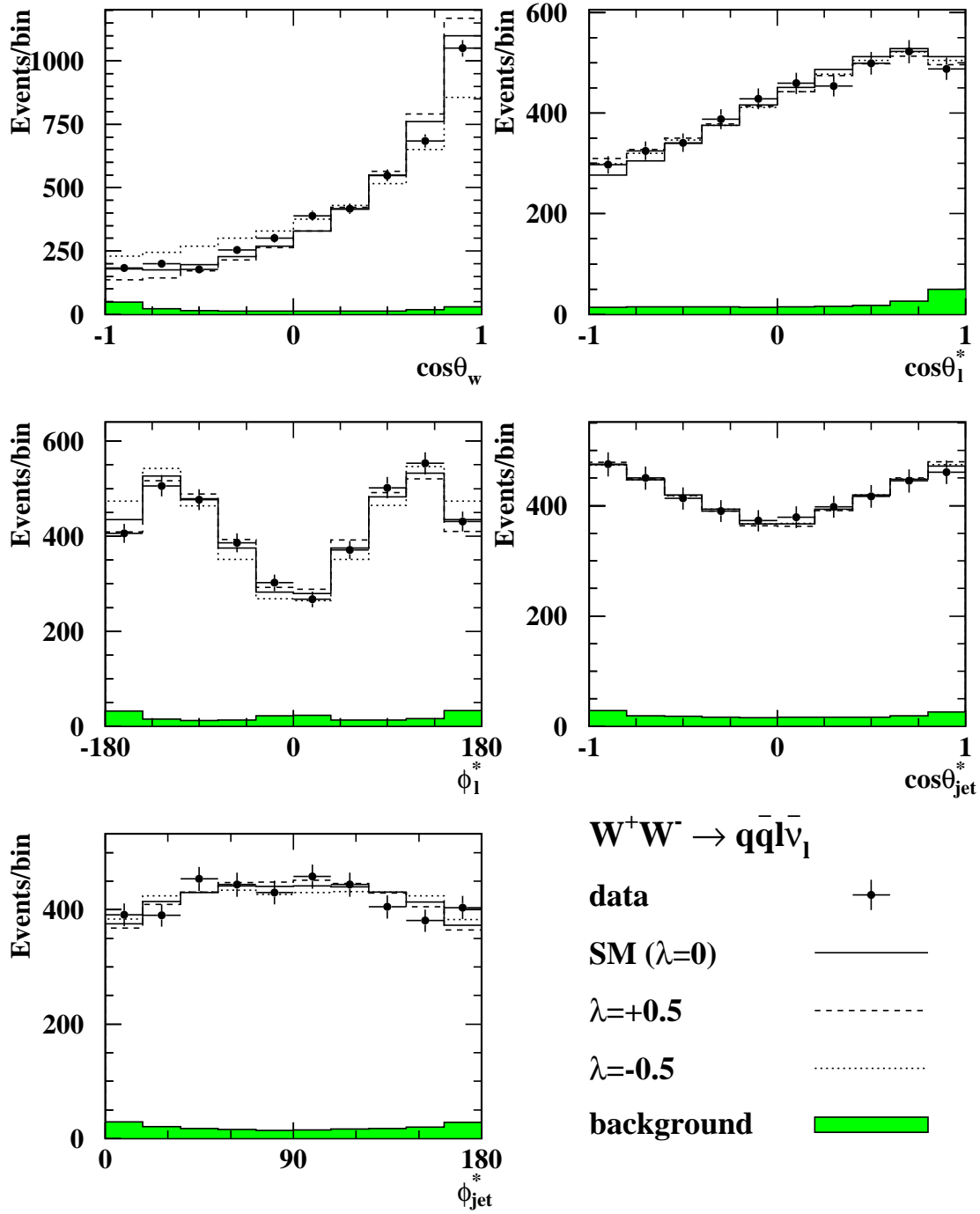


Figure 1: Distributions of the kinematic variables $\cos\theta_w$, $\cos\theta_{\ell}^*$, ϕ_{ℓ}^* , $\cos\theta_{jet}^*$ and ϕ_{jet}^* , obtained from the $q\bar{q}l\nu_{\ell}$ candidates. The solid points represent the data. The histograms show the Monte Carlo expectation of the Standard Model (solid line) and the cases of $\lambda = +0.5$ and $\lambda = -0.5$ (dashed and dotted lines respectively). The Monte Carlo histograms are normalised to the number of data events. The shaded histograms show the non- $q\bar{q}l\nu_{\ell}$ background. In the case of $W^+ \rightarrow \bar{\ell}\nu$ decays the value of ϕ_{ℓ}^* is shifted by 180° in order to overlay W^+ and W^- distributions in the same plot, which is valid so long as CP is conserved.

shaded histograms show the non- $q\bar{q}\ell\bar{\nu}_\ell$ background and their normalisation relative to the signal is according to the Standard Model. For the $\cos\theta_{\text{jet}}^*$ and ϕ_{jet}^* distributions the jet with $0 \leq \phi_{\text{jet}}^* \leq 180^\circ$ is arbitrarily chosen as the quark jet from the decay of the W^- , or the anti-quark jet from the decay of the W^+ . Sensitivity to λ is apparent mainly for $\cos\theta_W$. The contribution of $\cos\theta_\ell^*$, ϕ_ℓ^* , $\cos\theta_{\text{jet}}^*$ and ϕ_{jet}^* to the overall sensitivity enters mainly through their correlations with $\cos\theta_W$.

3.2 Reconstruction of $q\bar{q}q\bar{q}$ final states

Using the Durham k_\perp algorithm [36] each selected $q\bar{q}q\bar{q}$ candidate is reconstructed as four jets whose energies are corrected for double counting of charged track momenta and calorimeter energies [37]. These four jets can be paired into W-bosons in three possible ways. To improve the resolution on the jet four-momenta we perform the five-constraint kinematic fit B for each possible jet pairing. In the following we consider only good jet pairings, namely those pairings with a successful fit B yielding a W-mass between 70 and 90 GeV. We accept only events with at least one good jet pairing.

After this cut the overall efficiency is around 80%, varying slightly with the centre-of-mass energy, and the contamination from other W^+W^- decays is below 0.3%. The major background contribution is from $Z^0/\gamma \rightarrow q\bar{q}$ where additional quarks or gluons are radiated off the primary quarks. This contribution is between 12% to 17%, decreasing with centre-of-mass energy. The contribution of TGC-independent four-fermion final states is 4.5%, except at 183 GeV where it drops to 3%.

We use a jet charge method as an estimator for the W charge. For the two jets coming from one W candidate we calculate the momentum weighted charge of all tracks contributing to this W candidate as, $Q_W = \sum_{i=1}^{N_W} q_i |p_{||,i}|^{0.5} / \sum_{i=1}^{N_{\text{tot}}} |p_{||,i}|^{0.5}$, where N_W and N_{tot} are the numbers of tracks in the W candidate and in the total event respectively, q_i is the charge of the i^{th} track and $p_{||,i}$ is the momentum component parallel to the jet axis. We take the W candidate with the more positive charge as the W^+ .

Around 38% of the events have more than one good jet pairing, but the fraction of events where all three possible jet pairings are good is below 5%. To select the correct jet pairing, the good pairings in the event are processed through a likelihood algorithm [38] which takes into account correlations between the input variables. We use as input to our likelihood the W candidate mass as obtained from the kinematic fit B, the absolute value of the difference between the W candidate masses as obtained from the kinematic fit A and the absolute value of the jet charge difference between the two W candidates. The algorithm has been tuned on Monte Carlo events at each centre-of-mass energy in order to give the optimal performance. The di-jet pairing with the highest likelihood output is taken as the correct pairing. The distribution of the highest jet pairing likelihood output is shown in Figure 2(a). The distribution of the W charge separation for all highest likelihood pairings is shown in Figure 2(b).

According to the W^+W^- KORALW Monte Carlo, the probability of selecting the correct di-jet combination is about 80%, and the probability of correct assignment of the W charge, once the correct pairing has been chosen, is about 77%. Both probabilities vary slightly with the

OPAL

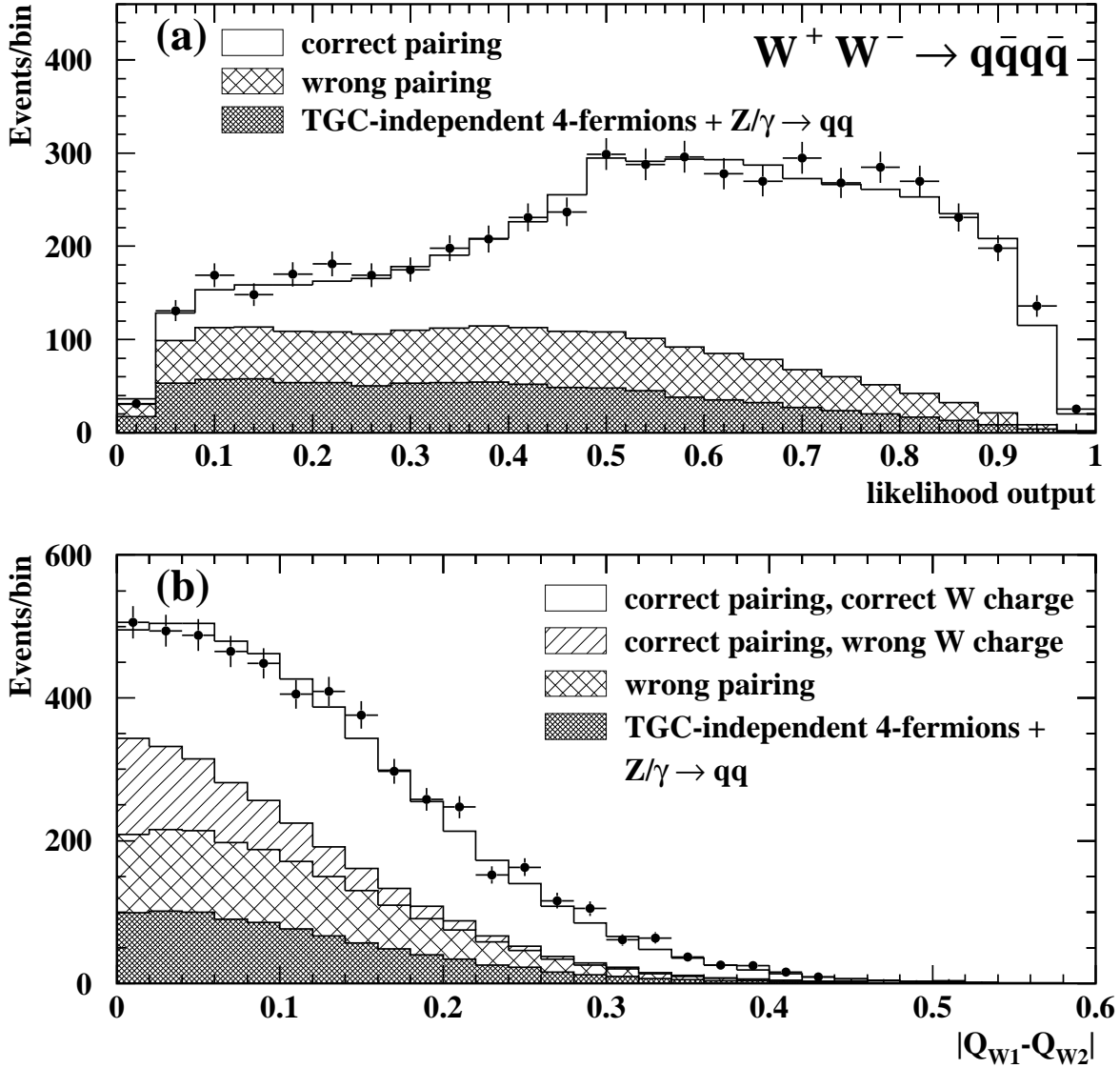


Figure 2: Distributions for $q\bar{q}q\bar{q}$ data events (points) for the *KandY* four-fermion Monte Carlo (histogram) of (a) jet-pairing likelihood corresponding to the most likely combination; (b) charge separation between the two W candidates.

centre-of-mass energy but depend strongly on the jet pairing likelihood output.

In order to reflect this dependence on the jet pairing likelihood output we use the output as a quality variable to classify the events into four quality classes which are later used in the TGC analysis. The definitions of these classes and the fraction of accepted events in each class are listed in Table 3. For classes with higher jet pairing likelihood output the probability for selecting the correct di-jet combination and the correct W charge assignment increases. The numbers are given in Table 3. The population of each class is well modelled by Monte Carlo.

Class	Jet pairing likelihood output	% of events	Correct jet pairing probability	Correct charge assignment probability
a)	0.72 - 1.00	27.2	91.8%	89.4%
b)	0.54 - 0.72	24.9	84.4%	74.1%
c)	0.35 - 0.54	22.4	75.3%	66.2%
d)	0.00 - 0.35	25.5	56.4%	67.9%

Table 3: Definition of the four quality classes of $q\bar{q}q\bar{q}$ events. The correct charge assignment probability is calculated only for those events with correct jet pairing.

The distributions of the variables $\cos\theta_W$, $\cos\theta_{\text{jet}}^*$ and ϕ_{jet}^* are shown in Figure 3, along with the expected distributions for the Standard Model ($\lambda=0$) and for $\lambda=\pm 0.5$. In the $\cos\theta_{\text{jet}}^*$ and ϕ_{jet}^* distributions there are two entries per event, and according to our convention (see Section 3.1), the jet with $0 \leq \phi_{\text{jet}}^* \leq 180^\circ$ is chosen as the quark jet from the decay of the W^- , or the anti-quark jet from the decay of the W^+ . The Monte Carlo histograms are normalised to the number of data events. The shaded histograms represent the separate contributions from wrong pairings, correct pairing but wrong charge and background. Their relative normalisation is according to the Standard Model. The data are again described well by the Standard Model prediction.

3.3 Reconstruction of $\ell\bar{\nu}_\ell\bar{\ell}'\nu_{\ell'}$ final states

The reconstruction of $\ell\bar{\nu}_\ell\bar{\ell}'\nu_{\ell'}$ final states is possible, using kinematic fit C, only if there is no τ -lepton in the final state. To reject events with τ -leptons we use the lepton identification algorithm designed for the W branching ratio measurement [34]. The event rate analysis selection sometimes selects events with only one high momentum charged lepton reconstructed in the detector: such events were removed from the angular distribution analysis as the momenta of both charged leptons must be measured. As a result of these two cuts, the efficiency for $\ell\bar{\nu}_\ell\bar{\ell}'\nu_{\ell'}$ events with $\ell, \ell' = e, \mu$ drops from $\sim 88\%$ to $\sim 73\%$, varying slightly with centre-of-mass energy. The contamination left in the sample from $\ell\bar{\nu}_\ell\bar{\ell}'\nu_{\ell'}$ final states with a τ -lepton is 14% and the background from other final states is 2%.

Kinematic fit C has zero constraints and reduces to solving a quadratic equation. In the ideal case of no measurement errors and satisfying the conditions where fit C is valid, namely no ISR and narrow W width, one expects to obtain two real solutions corresponding to a two-fold ambiguity in the angle set $\cos\theta_W$, ϕ_1^* and ϕ_2^* . There is no ambiguity in the angles θ_1^* and θ_2^* which have a one-to-one correspondence with the lepton momenta. In realistic conditions, however,

OPAL

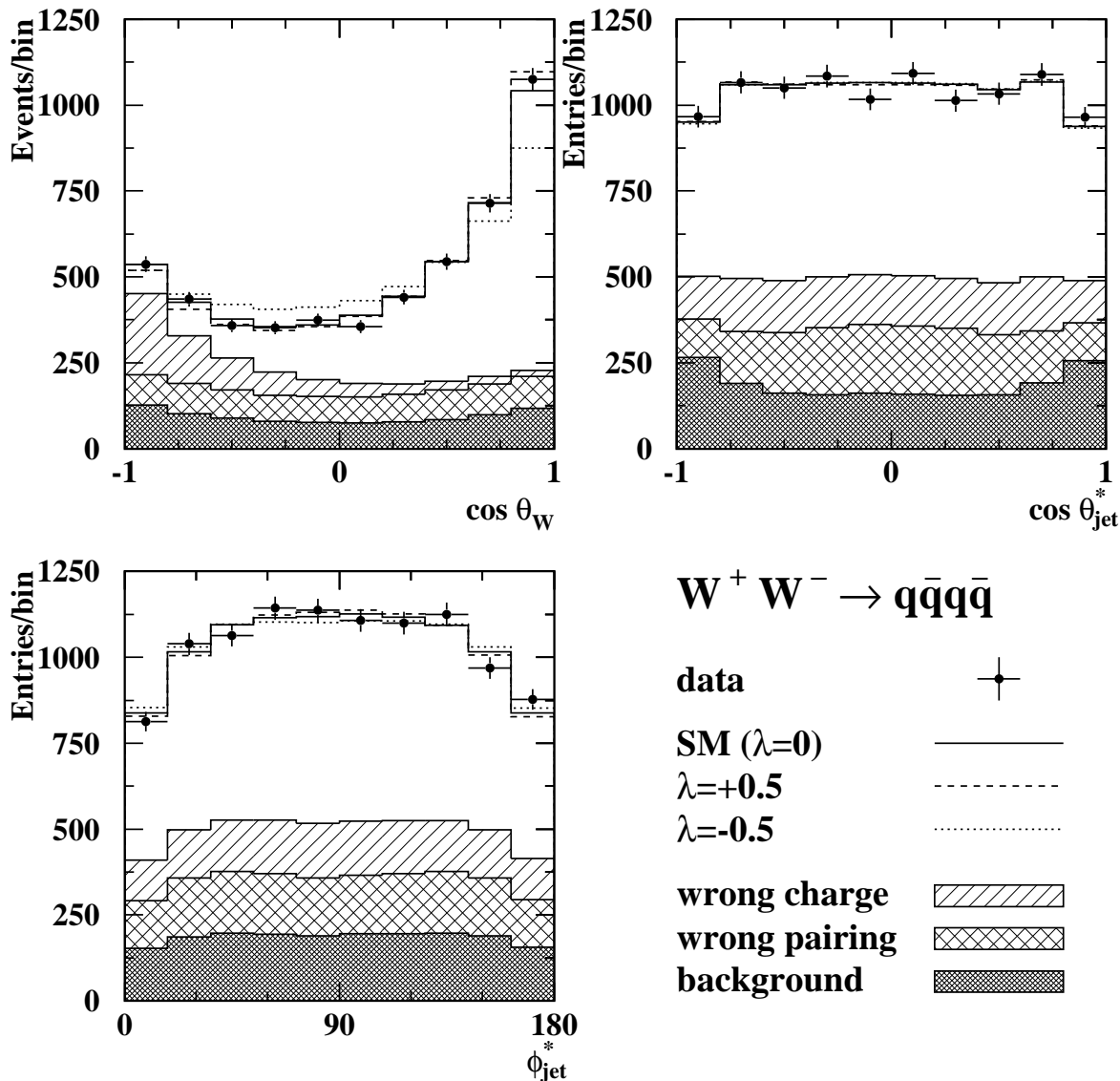


Figure 3: Distribution of the kinematic variables $\cos \theta_W$, $\cos \theta_{\text{jet}}^*$, and ϕ_{jet}^* for $q\bar{q}q\bar{q}$ events. In the $\cos \theta_{\text{jet}}^*$, and ϕ_{jet}^* distributions there are two entries per event. The solid points represent the data. The histograms show the Monte Carlo expectation of the Standard Model (solid line) and the cases of $\lambda=+0.5$ and $\lambda=-0.5$ (dashed and dotted lines respectively). The Monte Carlo histograms are normalised to the number of data events. The open histograms show the contribution from correct pairing and correct charge assignment. The single hatched histograms represent the contribution from correct pairing, but wrong charge assignment. The cross-hatched histograms correspond to the contribution from wrong pairing, and the dark histograms show the contribution of background.

including ISR, finite W width and measurement errors, one may obtain no real solution, but a pair of complex conjugate solutions. The fraction of events with complex solutions falls with increasing centre-of-mass energy from 30% to 24%, in agreement with Monte Carlo prediction. In these events, the imaginary parts of the complex solutions are set to zero, yielding a single real angle set. The total weight of all events is the same, independent of whether one or two solutions are employed. In the latter case, the two solutions each are assigned a weight of one half.

Figure 4 shows the distributions of the five reconstructed angles and the expected distributions for $\lambda=0, \pm 1$. The Monte Carlo histograms are normalized to the number of data events. The shaded histograms represent the contribution of background and their normalisation relative to the signal is according to the Standard Model. The data distributions agree with the expectation of the Standard Model.

4 Optimal observable analysis

The angular distributions from all final states are consistent with the Standard Model expectation and no evidence is seen for any significant contributions from anomalous couplings. For a quantitative study we use the method of optimal observables in the same way as in [4]. This method relies on the linear dependence of the triple gauge vertex Lagrangian on the TGCs, corresponding to a second-order polynomial dependence of the differential cross-section,

$$\frac{d\sigma(\Omega, \alpha)}{d\Omega} = S^{(0)}(\Omega) + \sum_i \alpha_i \cdot S_i^{(1)}(\Omega) + \sum_{i,j} \alpha_i \alpha_j \cdot S_{ij}^{(2)}(\Omega), \quad \alpha_i = \Delta\kappa_\gamma, \Delta g_1^z, \lambda \text{ and } g_5^z,$$

where $S^{(0)}$, $S_i^{(1)}$ and $S_{ij}^{(2)}$ are functions of the five phase-space variables, $\Omega=(\cos\theta_W, \cos\theta_1^*, \phi_1^*, \cos\theta_2^*, \phi_2^*)$. For this kind of dependence it has been shown [39] that all information contained in the phase-space variables Ω , which is relevant to the four couplings, is retained in the whole set of 14 observables $\mathcal{O}_i^{(1)} = S_i^{(1)}(\Omega)/S^{(0)}(\Omega)$, $\mathcal{O}_i^{(2)} = S_{ii}^{(2)}(\Omega)/S^{(0)}(\Omega)$ and $\mathcal{O}_{ij}^{(2)} = \mathcal{O}_{ji}^{(2)} = S_{ij}^{(2)}(\Omega)/S^{(0)}(\Omega)$ ($i, j = 1, 2, 3, 4$). In this analysis we use the mean values of $\mathcal{O}_i^{(2)}$ and $\mathcal{O}_{ij}^{(2)}$ in addition to the mean values of $\mathcal{O}_i^{(1)}$ [40].

In the one-parameter fit of α_i we only use the corresponding first order, $\mathcal{O}_i^{(1)}$, and second order, $\mathcal{O}_i^{(2)}$, observables. In this way, the other couplings are not used in the fit. Similarly, in two-parameter fits where two couplings are allowed to vary simultaneously, we use only the five observables corresponding to these couplings and their mutual correlations. When three couplings are allowed to vary, nine observables are used.

The calculation of the mean optimal observables and their expected values is done separately for each centre-of-mass energy and for each of the $q\bar{q}\ell\bar{\nu}_\ell$, $q\bar{q}q\bar{q}$ and $\ell\bar{\nu}_\ell\bar{\ell}'\nu_{\ell'}$ final states. The optimal observables are constructed for each event k with the set of phase-space variables Ω_k using the analytic expression for the CC03 Born differential cross-section to calculate the values of $S^{(0)}(\Omega_k)$, $S_i^{(1)}(\Omega_k)$, $S_{ii}^{(2)}(\Omega_k)$ and $S_{ij}^{(2)}(\Omega_k)$. This calculation takes into account the reconstruction ambiguities for each particular final state. For the $q\bar{q}q\bar{q}$ channel, the ambiguity in the W -charge determination is taken into account by weighting the $S^{(0)}$, $S_i^{(1)}$ and $S_{ij}^{(2)}$ functions

for each charge hypothesis with the corresponding probability. This probability is determined from the Monte Carlo as a function of the estimated charge difference $|Q_{W_1} - Q_{W_2}|$ between the two W candidates in the event.

For $q\bar{q}\ell\bar{\nu}_\ell$ and $q\bar{q}q\bar{q}$ events the mean optimal observables are calculated using weights assigned to the event according to its quality class (see Tables 2 and 3). For $q\bar{q}\ell\bar{\nu}_\ell$ events, the weight for a particular class is inversely proportional to the variance of the optimal observable distribution of the events in that class. For $q\bar{q}q\bar{q}$ events, the weights are calculated in a similar way, using the variances of the optimal observable *resolution* distributions. In this way, events where the quality of the reconstruction is poor obtain a lower weight. Using this weighted mean has been found, as expected, to enhance our sensitivity.

The expected mean values of each observable as a function of the TGCs are calculated from four-fermion reference Monte Carlo samples generated according to the Standard Model. The EXCALIBUR matrix element calculation is used to reweight the Monte Carlo events to any TGC value required. The contribution of background events is also taken into account in the calculation of the expected mean values using corresponding Monte Carlo samples.

A χ^2 fit of the measured mean values $\bar{\mathcal{O}}$ to the corresponding expectations $E[\mathcal{O}](\alpha)$ is performed to extract the couplings from the data. The covariance matrix for the mean values is calculated from the Monte Carlo events and scaled to the number of data events.

In some of our fits the χ^2 function has a double minimum and therefore it is necessary to validate the errors obtained from the χ^2 fits. This is performed with a large number of Monte Carlo “experiments”. In each of these “experiments”, we use for each centre-of-mass energy and each final state a subsample of Standard Model Monte Carlo events. The size of each subsample corresponds to the luminosity for that final state at the particular centre-of-mass energy. Background events are also included in these subsamples in the appropriate proportions. For each “experiment”, the various subsamples are analysed in the same way as the real data events. The distributions of the fit results are centred around the expected values, but there are some non-Gaussian tails. We therefore test the reliability of the error interval, as given by the region where χ^2 is no more than 1 above its minimum value, by counting the fraction of “experiments” where the correct value falls within this region. The error estimate is considered to be reliable if the calculated fraction is consistent with 68%; otherwise the corresponding elements of the covariance matrix for the $\bar{\mathcal{O}}$ values are scaled up by the necessary factor to obtain 68% of the subsamples within the error interval. The resulting scaled covariance matrix is also used to analyse the real data. This is done separately for each fit. The resulting scale factors vary between 1 and 1.076 for the one-parameter fits. However, in the three-parameter fit of $\Delta\kappa_\gamma$, Δg_1^Z and λ , where double minima occur more frequently, a larger scale factor of 1.28 is obtained. These scale factors have been found to be appropriate also for the 95% C.L. intervals.

5 Systematic errors in the angular distribution analysis

The following sources of systematic uncertainty are considered, as listed in Table 4.

- a) There is a theoretical uncertainty in the $\mathcal{O}(\alpha)$ correction due to missing higher orders in the YFSWW3 Monte Carlo generator program. As a conservative estimate of this uncertainty, this $\mathcal{O}(\alpha)$ correction is removed, degrading the events to KORALW1.42 level. The effect of this change is taken as a systematic uncertainty.
- b) KORALW includes ISR up to $\mathcal{O}(\alpha^3)$. As a conservative estimate of missing higher orders, we replace it with ISR up to $\mathcal{O}(\alpha)$ only and take the difference as a systematic uncertainty.
- c) Another uncertainty in the signal Monte Carlo generator is related to the PYTHIA fragmentation and hadronisation model which is used. To study the effect of this uncertainty we compare results of the analysis when applied to W^+W^- Monte Carlo samples generated with KORALW1.42 using either PYTHIA, HERWIG or ARIADNE for the fragmentation and hadronisation phase. The effect of changing to HERWIG is the larger and is used to estimate the uncertainty. The main effect is on the $q\bar{q}q\bar{q}$ final state, where HERWIG predicts a higher probability of correct jet pairing and correct W charge assignment than PYTHIA. This effect is partially due to the average charged multiplicity for light quarks being lower in our tuned version of HERWIG than in PYTHIA. Since the data are in agreement with PYTHIA [41], we weight the HERWIG Monte Carlo events so as to reproduce the same charged multiplicity distribution as PYTHIA. The effect of this weighting is a reduction of the systematic error by about 15-30%.
- d) To assess the uncertainty in the TGC matrix element calculation which is used to weight our Monte Carlo events, we replace the calculation from the EXCALIBUR Monte Carlo generator program with the one from `grc4f`.
- e) The Monte Carlo simulation of the OPAL detector has been studied using back-to-back jets and leptons in Z^0 events collected during calibration runs which were taken regularly every year between the high energy runs. Some scaling and smearing had to be applied to the reconstructed jets and leptons in the Monte Carlo in order to achieve the best agreement with data. The uncertainties in these corrections correspond to variations in our results which are taken as systematic errors. These corrections are usually applied *after* the event selection. To estimate their effect on the selection of our sample, they were applied as a systematic check *before* the event selection, and the difference from the standard result was added in quadrature with the effects of the uncertainties on the corrections.
- f) Uncertainties in the background estimation are determined by varying both its shape and normalisation. To study the effect of the shape we use alternative samples for each background source, keeping the normalisation fixed. For the TGC-independent four-fermion background we use EXCALIBUR and `grc4f` instead of KORALW. For the $Z^0/\gamma \rightarrow q\bar{q}$ background we use KK2F with HERWIG or ARIADNE rather than PYTHIA fragmentation. Finally, the HERWIG two-photon samples are replaced with F2GEN. For the background normalisation uncertainty the contribution from each source is scaled, one at a time, by the factors 1.2, 1.3 and 2.0 respectively. These scale factors are determined from studies with control data samples and from the differences between the alternative Monte Carlo generators, as explained in [34].
- g) The consequences of the uncertainties in the centre-of-mass energy and the W mass are estimated as follows. For the centre-of-mass energy uncertainty of 40 MeV, Monte Carlo

samples at different centre-of-mass energies are used as pseudo-data. For the W mass we assume $M_W=80.456\pm 0.059$ GeV/ c^2 [35] which is 0.126 GeV/ c^2 higher than the one used in our Monte Carlo generators. We do not correct our TGC fit result for this shift in M_W , but it is accounted for in our systematic error, along with the M_W measurement error. The combined effect is assessed using Monte Carlo samples generated with different W masses.

- h) Bose-Einstein correlations (BEC) in $q\bar{q}q\bar{q}$ events might affect the reconstruction of the W bosons and measured W charge distribution. We investigate this effect with a Monte Carlo program simulating BEC via re-adjustment of final state momenta using the LUBOEI model [42]. When both inter- W and intra- W correlations are taken into account, the bias is found to be larger than the case where only intra- W boson correlations are present.
- i) The jet reconstruction and the measured W charge distribution in $q\bar{q}q\bar{q}$ events might also be affected by colour reconnection. This effect is investigated with several MC samples generated according to the Sjöstrand-Khoze [43] models. We consider model I with colour reconnection probabilities of 34% and 97%. Models II and II' are also considered. Model I with colour reconnection probability of 97% produces the largest bias.

The Monte Carlo samples are larger than the data by a factor of 150 - 900, depending on the centre-of-mass energy. Therefore, the uncertainty due to Monte Carlo statistics is neglected.

The effect of each of these sources on the mean values of the optimal observables is estimated separately for each centre-of-mass energy and for each final state. The deviations obtained in the mean observables are used to construct a systematic error covariance matrix, where the systematic deviations from each source are assumed to be fully correlated between all centre-of-mass energies. For the combination of all final states, the covariance matrix is extended to incorporate the three final states. All uncertainties, except for those associated with the background, are assumed to be fully correlated between the relevant final states. This matrix is added to the statistical covariance matrix, and the fit is redone to obtain the TGC parameters with their total (statistical and systematic) errors.

Source	$\Delta\kappa_\gamma$	Δg_1^z	λ	g_5^z
a) $\mathcal{O}(\alpha)$ correction	0.029	0.011	0.010	0.031
b) ISR	0.006	0.002	0.003	0.003
c) Fragmentation	0.038	0.013	0.018	0.047
d) TGC matrix element	0.011	0.005	0.004	0.005
e) Detector simulation	0.006	0.003	0.005	0.013
f) Background	0.015	0.004	0.011	0.012
g) \sqrt{s} , M_W	0.008	0.004	0.005	0.017
h) Bose-Einstein correlations	0.001	0.000	0.004	0.005
i) Colour reconnection	0.004	0.003	0.005	0.000
Total	0.053	0.019	0.026	0.061

Table 4: Contributions to the systematic uncertainties in the determination of the TGC parameters. The total systematic errors are obtained by combining all contributions at the optimal observable level and then calculating the effect on the TGC parameters.

For demonstration, we also calculate the separate contribution from each source of systematic error to the error on the TGC parameters, after combining the different centre-of-mass energies and final states. These are listed in Table 4.

6 Event rate TGC analysis

The event rate study, unlike the angular distribution analysis, requires a detailed investigation of the systematic uncertainties associated with the overall selection efficiency. This investigation is part of the W -pair cross-section analysis and has to be done separately for each centre-of-mass energy and for each final state. So far, it has been completed for centre-of-mass energies of 183 GeV [3] and 189 GeV [34]. The TGC event rate analysis is therefore also restricted to these two centre-of-mass energies. In the case where the angular distribution analysis has two TGC solutions, one being far away from the Standard Model value, the results from this restricted event rate analysis would still be sufficient to reject that solution. The data from higher centre-of-mass energies would make a negligible additional contribution to our results. Compared with the angular distributions, the sensitivity of the event rates to TGCs around the Standard Model values is much smaller and its dependence on the overall luminosity is weaker.

The event rate analysis has been described already in our previous publications [3, 4]. The numbers of expected events are re-evaluated for this analysis using the KandY Monte Carlo samples to obtain the Standard Model expected number of events.

The same selection, efficiency and background estimates as in the total cross-section analysis are used here. The numbers of selected events in each final state and for each of the two centre-of-mass energies are quoted in Table 5 along with the Monte Carlo expectations. The systematic errors on the expected values are due to Monte Carlo statistics, 0.5% uncertainty in the total cross-section, 0.2% uncertainty in the luminosity, uncertainties due to data/MC differences, tracking losses, detector occupancy and fragmentation. A detailed description of all these sources can be found in [34]. The expected numbers of signal events include contributions from all four-fermion final states which can be produced by diagrams involving the $WW\gamma$ and WWZ triple gauge boson vertices. The other four-fermion final states are considered as background along with the two-fermion final states and two-photon processes.

\sqrt{s} (GeV)	Luminosity (pb^{-1})	Final state	Observed events	Expected events		
				Total	Signal	Background
182.7	57.21 ± 0.25	$\ell\bar{\nu}_\ell\bar{\ell}\nu_\ell$	78	77.5 ± 3.1	76.1 ± 2.2	1.4 ± 2.2
		$q\bar{q}\ell\bar{\nu}_\ell$	361	364 ± 6	337 ± 6	27 ± 3
		$q\bar{q}q\bar{q}$	438	436 ± 10	344 ± 5	92 ± 9
188.6	183.05 ± 0.40	$\ell\bar{\nu}_\ell\bar{\ell}\nu_\ell$	276	287.2 ± 5.0	272.6 ± 4.1	14.6 ± 2.9
		$q\bar{q}\ell\bar{\nu}_\ell$	1246	1248 ± 16	1171 ± 13	76 ± 10
		$q\bar{q}q\bar{q}$	1546	1497 ± 26	1189 ± 14	309 ± 21

Table 5: Observed and expected numbers of events in each W^+W^- final state for the centre-of-mass energies of 182.7 GeV and 188.6 GeV. The separation between signal and background is explained in the text. All the quoted errors are systematic.

The total numbers of expected events are consistent within the statistical and systematic errors with the observed numbers. Therefore, there is no evidence for any significant contribution from anomalous couplings. A quantitative study of TGCs from these results is performed by comparing the numbers of observed events in each of the three event selection channels at each of the two centre-of-mass energies with the expected numbers of signal and background events, where the number of signal events is parametrised as a second-order polynomial in the TGCs. This parametrisation is based on the second-order polynomial dependence of the cross-section, as was used also in the optimal observable analysis (see Section 4). The polynomial coefficients in terms of event rate for each final state are calculated by weighting our Monte Carlo events to correspond to various TGC values using a four-fermion matrix element calculation procedure taken from the EXCALIBUR Monte Carlo generator program.

The probability to observe the measured number of candidates, given the expected value, is calculated using a Gaussian distribution where the errors also include the systematic uncertainties. We assume full correlation between the systematic uncertainties for the three final states except for efficiency and background which are taken to be uncorrelated. All systematic uncertainties are assumed to be fully correlated between the two different centre-of-mass energies.

7 Combined TGC results

The results of the various fits are listed in Table 6. We present first the results of the angular distribution analysis without systematic errors obtained by performing one-parameter fits for each final state simultaneously for the eight centre-of-mass energies. For comparison, the average fit errors of the Monte Carlo “experiments” are also quoted in Table 6, demonstrating the different sensitivities for the various final states and TGC parameters. In most cases, the fit errors are rather close to the expected ones, except for $\Delta\kappa_\gamma$, where the fit errors for some final states are also very asymmetric due to the proximity of a second minimum in the χ^2 function.

Next we present the results of the angular distribution analysis with the systematic errors included as explained in Section 5. This modifies the relative contributions to the fit of the different optimal observables and different centre-of-mass energies, as well as the correlations between them. Therefore, not only the fit errors are affected, but also the fit results themselves. The corresponding $\log L$ curves⁵ for the different channels are shown in Figure 5. The results from the three final states are combined, taking into account the common systematic errors as explained in Section 5, and the combined results are listed in Table 6.

The results of the event rate analysis are presented by $\log L$ curves shown by the thin solid lines in Figure 5. They are combined with the results of the angular distribution analysis and the combined $\log L$ plots are shown by the thick solid lines. The correlation between the results of the two analyses, which is due to uncertainties in the background normalisation, centre-of-mass energy and W mass, is below 7%. Therefore this correlation is neglected in the combination. The numerical results of the combination are listed in Table 6 along with the corresponding $\chi^2/\text{d.o.f.}$ As expected, the event rate information has relatively little impact on the final results.

⁵Following the convention in LEP, we prefer to display our results by the logarithm of the likelihood function, $\log L$, related to the χ^2 function by, $-\log L = \chi^2/2$. The plotted function is $-\Delta\log L$, which is obtained by subtracting from $-\log L$ its minimum value.

	$\Delta\kappa_\gamma$	Δg_1^z	λ	g_5^z
<u>$q\bar{q}\ell\bar{\nu}_\ell$</u>				
Without systematics	$-0.23_{-0.08}^{+0.09}$	$-0.031_{-0.034}^{+0.035}$	$-0.075_{-0.035}^{+0.036}$	$0.15_{-0.16}^{+0.16}$
Expected errors	± 0.12	± 0.032	± 0.033	± 0.15
Including systematics	$-0.23_{-0.08}^{+0.09}$	$-0.023_{-0.037}^{+0.038}$	$-0.062_{-0.037}^{+0.038}$	$0.10_{-0.16}^{+0.17}$
Fit χ^2 /d.o.f.	10.3/15	13.6/15	13.3/15	14.7/15
<u>$q\bar{q}q\bar{q}$</u>				
Without systematics	$0.18_{-0.20}^{+0.38}$	$0.08_{-0.07}^{+0.09}$	$0.00_{-0.07}^{+0.09}$	$-0.41_{-0.21}^{+0.20}$
Expected errors	± 0.20	± 0.07	± 0.08	± 0.20
Including systematics	$0.17_{-0.26}^{+0.65}$	$0.09_{-0.09}^{+0.11}$	$0.01_{-0.14}^{+0.28}$	$-0.37_{-0.25}^{+0.24}$
Fit χ^2 /d.o.f.	11.3/15	9.2/15	11.0/15	8.8/15
<u>$\ell\bar{\nu}_\ell\bar{\ell}\nu_\ell$</u>				
Without systematics	$0.31_{-0.27}^{+0.34}$	$-0.05_{-0.11}^{+0.11}$	$-0.09_{-0.08}^{+0.09}$	$0.12_{-0.44}^{+0.48}$
Expected errors	± 0.29	± 0.13	± 0.09	± 0.34
Including systematics	$0.30_{-0.28}^{+0.35}$	$-0.06_{-0.11}^{+0.11}$	$-0.09_{-0.08}^{+0.09}$	$0.10_{-0.45}^{+0.49}$
Fit χ^2 /d.o.f.	14.6/15	12.9/15	9.8/15	14.9/15
<u>All WW final states</u>				
Including systematics	$-0.12_{-0.08}^{+0.09}$	$-0.013_{-0.033}^{+0.034}$	$-0.061_{-0.034}^{+0.035}$	$-0.04_{-0.12}^{+0.13}$
Including event rate	$-0.12_{-0.08}^{+0.09}$	$-0.013_{-0.033}^{+0.034}$	$-0.060_{-0.033}^{+0.034}$	$-0.04_{-0.12}^{+0.13}$
Fit χ^2 /d.o.f.	43.4/53	39.4/53	36.2/53	42.0/53
Standard Model χ^2 /d.o.f.	45.1/54	39.5/54	39.2/54	42.1/54
95% C.L. limits	$[-0.27, 0.07]$	$[-0.077, 0.054]$	$[-0.13, 0.01]$	$[-0.28, 0.21]$

Table 6: Measured values of the TGC parameters from the angular distributions of each WW final state, using centre-of-mass energies of 183 – 209 GeV and the results after combining all final states. For the individual final states we also list the results before including the systematic errors and the expected statistical errors. We also list the results after combining with the W-pair event rate information from centre-of-mass energies of 183 and 189 GeV. The quality of the fits is demonstrated by their respective χ^2 values and numbers of degrees of freedom. The compatibility with the Standard Model is shown by the χ^2 values obtained when the TGCs assume their Standard Model values.

OPAL

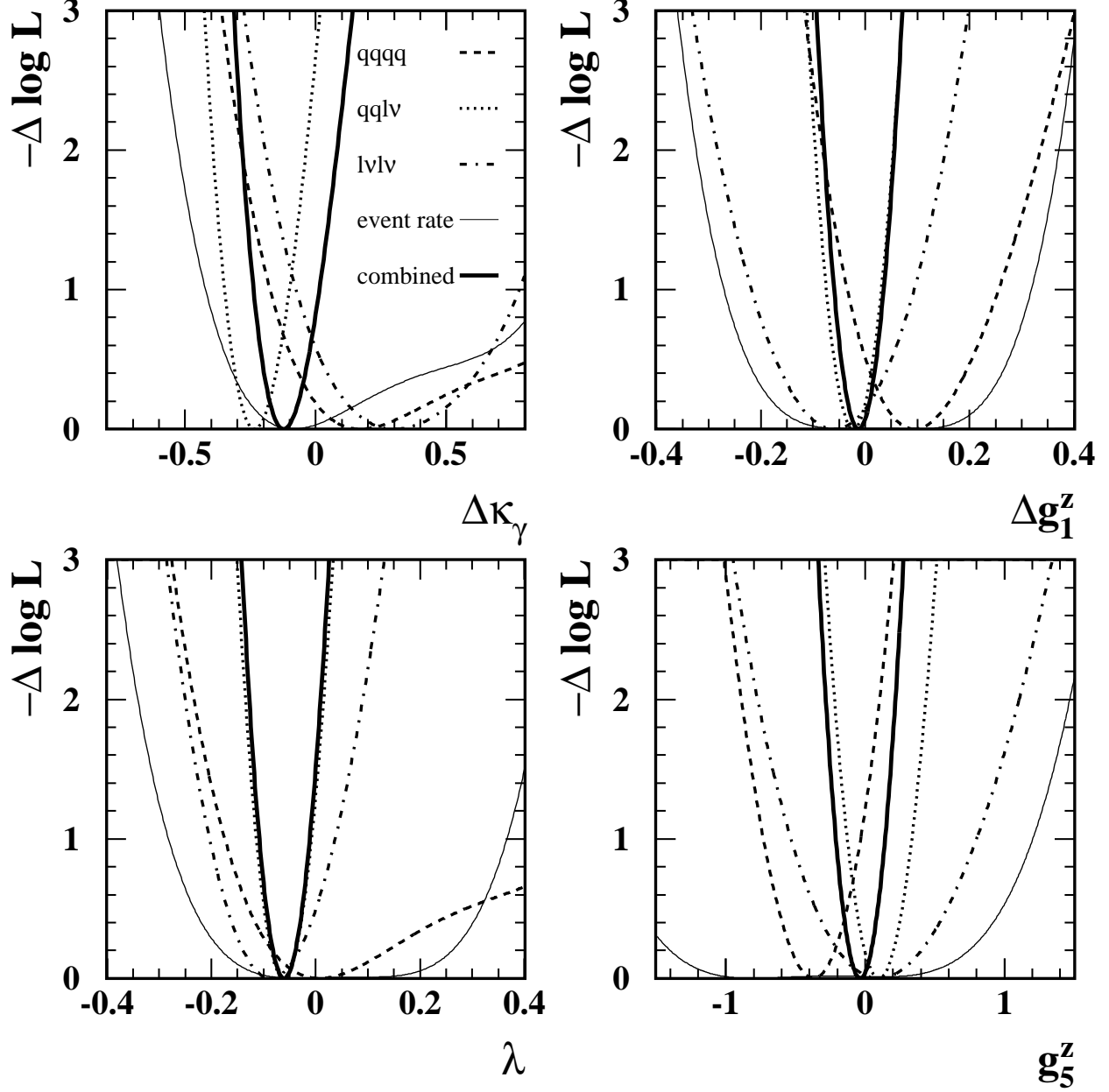


Figure 5: Negative log-likelihood curves obtained from the angular distribution information of W -pair events taken at the centre-of-mass energies of 183 – 209 GeV, separately for the three different final states: $q\bar{q}\ell\nu_\ell$ (dotted lines), $q\bar{q}q\bar{q}$ (dashed lines) and $\ell\nu_\ell\bar{\ell}\nu_\ell$ (dash-dotted lines). The thin solid lines describe the contribution of the event rate information from all final states corresponding to centre-of-mass energies of 183 and 189 GeV. The systematic errors are included. The thick solid lines are obtained by combining all sources of information. The curves for each TGC parameter are obtained by setting the other three parameters to their Standard Model values.

The 95% confidence level intervals are also listed in Table 6. To show the compatibility with the Standard Model we also list in the table the $\chi^2/\text{d.o.f.}$ for Standard Model TGC values.

To study correlations between the C- and P-conserving TGC parameters, $\Delta\kappa_\gamma$, Δg_1^z and λ , we perform fits where two parameters are allowed to vary while the third parameter and g_5^z assume their Standard Model values and are not used in the fit, as explained in Section 4. Similarly, we also perform a three-parameter fit where all three parameters are allowed to vary, leaving out only g_5^z . Figure 6 shows the 95% C.L. contour plots obtained from the two-parameter fits and the corresponding two-dimensional projections of the three-parameter fit. The contour plots show a double minimum structure. Adding information from the single W channel, where the $-\log L$ function tends to have a steep rise with increasing $\Delta\kappa_\gamma$ [6], is expected to resolve this ambiguity.

A χ^2 test can be used to study the compatibility of our data with the Standard Model, in the same way as was done for the one parameter fits. Inserting the Standard Model values for the TGC parameters we obtain $\chi^2 = 211.6$ for 222 degrees of freedom.

8 Summary

Using a sample of W^+W^- candidates collected at LEP at centre-of-mass energies of 183 – 209 GeV, we measure the CP-conserving triple gauge boson couplings κ_γ , g_1^z , λ and g_5^z . For this measurement we use both the angular information of W-pair events and their total event rate. The results obtained are:

$$\begin{aligned}\kappa_\gamma &= 0.88_{-0.08}^{+0.09}, \\ g_1^z &= 0.987_{-0.033}^{+0.034}, \\ \lambda &= -0.060_{-0.033}^{+0.034}, \\ g_5^z &= -0.04_{-0.12}^{+0.13},\end{aligned}$$

where each parameter is determined from a single-parameter fit, while the other three parameters assume their Standard Model values. These results supersede those from our previous publications [1–4]. They are all consistent with the Standard Model predictions of 1, 1, 0 and 0 respectively. This measurement constitutes strong evidence for the gauge structure of the Standard Model.

Acknowledgements:

We particularly wish to thank the SL Division for the efficient operation of the LEP accelerator at all energies and for their close cooperation with our experimental group. In addition to the support staff at our own institutions we are pleased to acknowledge the
 Department of Energy, USA,
 National Science Foundation, USA,
 Particle Physics and Astronomy Research Council, UK,

OPAL

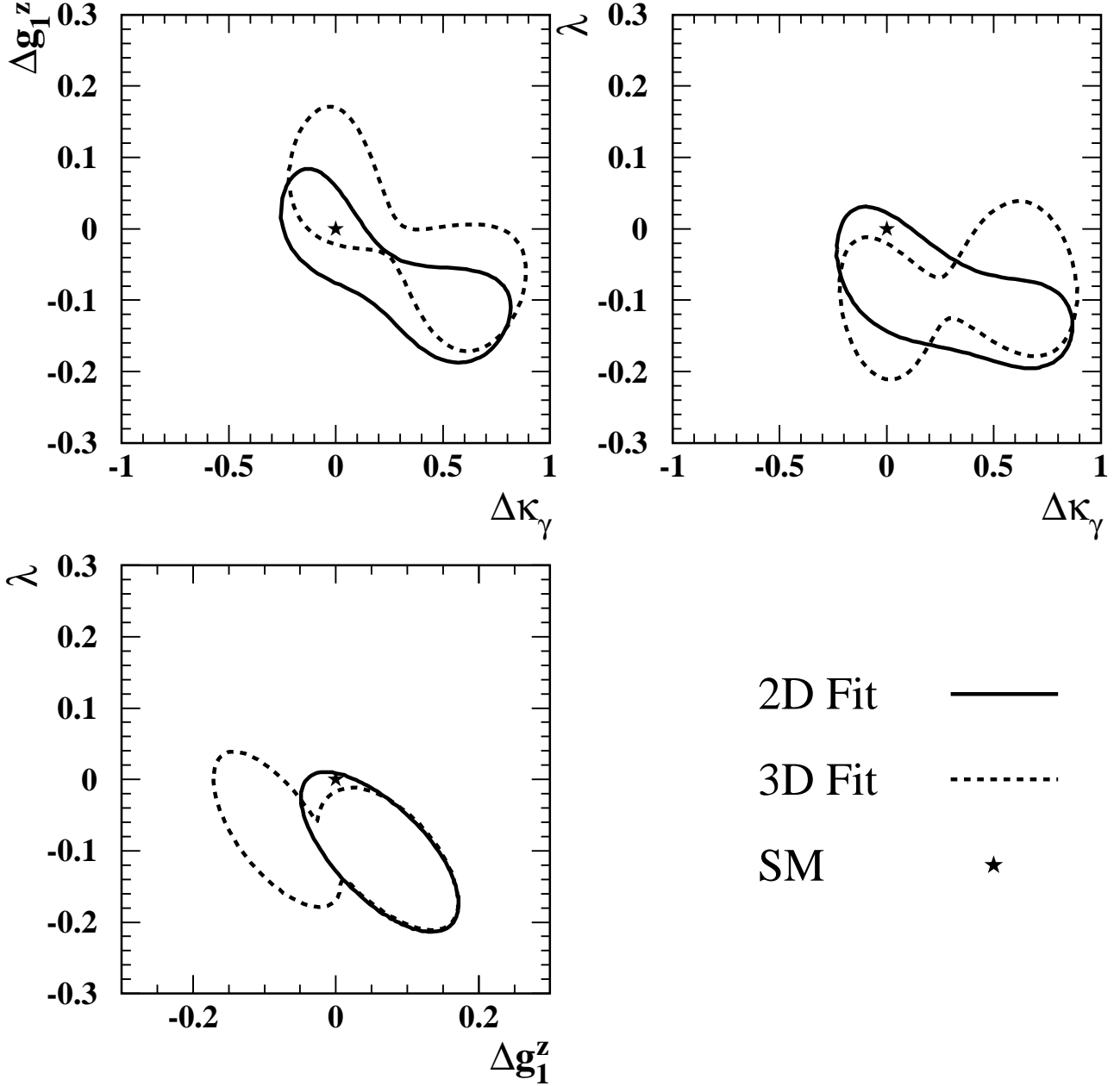


Figure 6: The two-dimensional correlation contours corresponding to $-\Delta \log L = 2.995$ for different pairs of TGC parameters, as obtained from two-parameter (solid curves) and three-parameter (dashed curves) fits. The value 2.995 corresponds to a 95% C.L. region in two dimensions. In the case of the three-parameter fit, the curve is a projection onto the two-dimensional plane of the envelope of the three-dimensional $-\Delta \log L = 2.995$ surface. The stars indicate the Standard Model expectations.

Natural Sciences and Engineering Research Council, Canada,
Israel Science Foundation, administered by the Israel Academy of Science and Humanities,
Benozio Center for High Energy Physics,
Japanese Ministry of Education, Culture, Sports, Science and Technology (MEXT) and a grant
under the MEXT International Science Research Program,
Japanese Society for the Promotion of Science (JSPS),
German Israeli Bi-national Science Foundation (GIF),
Bundesministerium für Bildung und Forschung, Germany,
National Research Council of Canada,
Hungarian Foundation for Scientific Research, OTKA T-038240, and T-042864,
The NWO/NATO Fund for Scientific Research, the Netherlands.

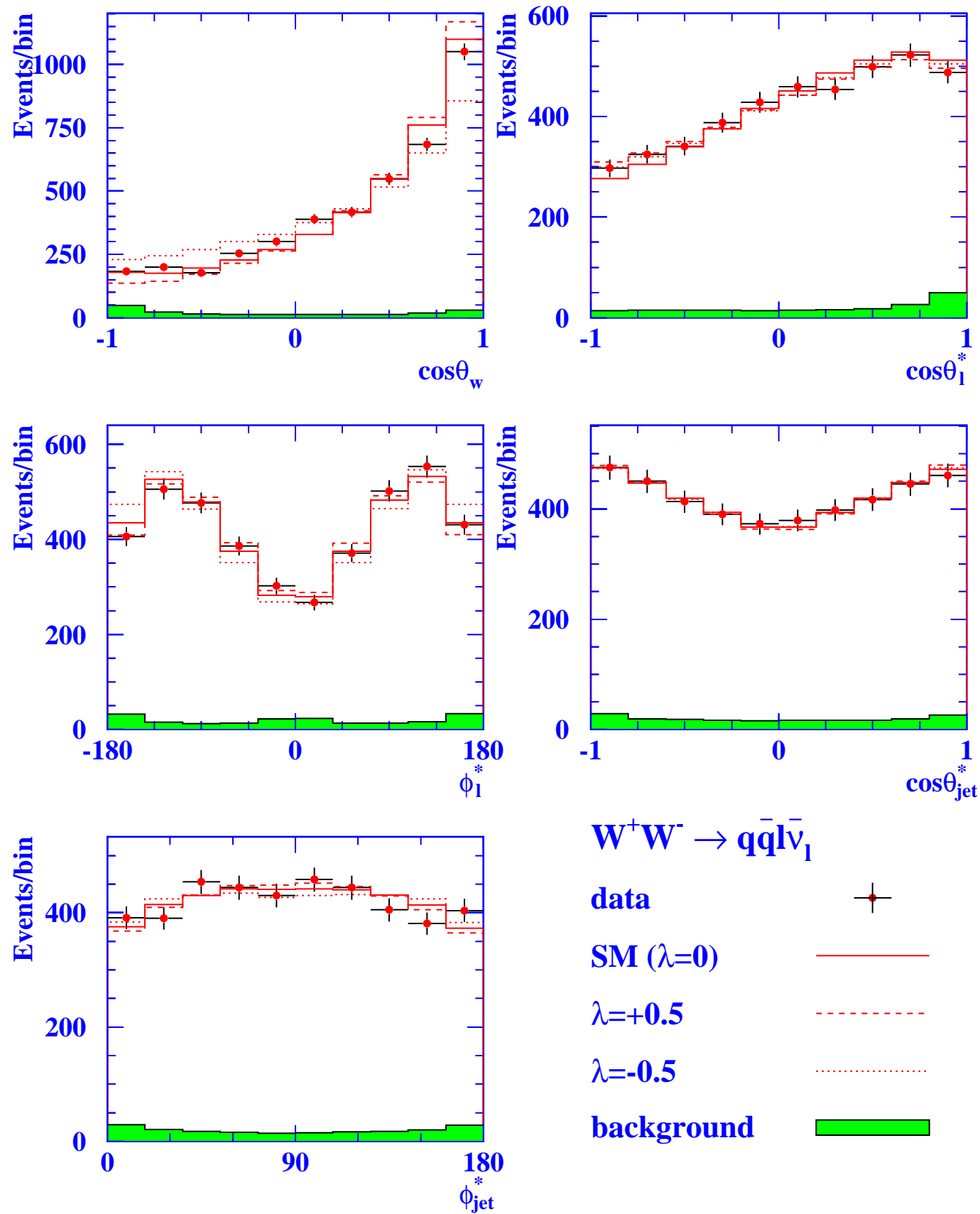
References

- [1] OPAL Collaboration, K. Ackerstaff *et al.*, Phys. Lett. **B397** (1997) 147.
- [2] OPAL Collaboration, K. Ackerstaff *et al.*, Eur. Phys. J. **C2** (1998) 597.
- [3] OPAL Collaboration, G. Abbiendi *et al.*, Eur. Phys. J. **C8** (1999) 191.
- [4] OPAL Collaboration, G. Abbiendi *et al.*, Eur. Phys. J. **C19** (2001) 1.
- [5] DELPHI Collaboration, P. Abreu *et al.*, Phys. Lett. **B397** (1997) 158;
L3 Collaboration, M. Acciarri *et al.*, Phys. Lett. **B398** (1997) 223;
L3 Collaboration, M. Acciarri *et al.*, Phys. Lett. **B413** (1997) 176;
DELPHI Collaboration, P. Abreu *et al.*, Phys. Lett. **B423** (1998) 194;
ALEPH Collaboration, R. Barate *et al.*, Phys. Lett. **B422** (1998) 369;
DELPHI Collaboration, P. Abreu *et al.*, Phys. Lett. **B459** (1999) 382;
L3 Collaboration, M. Acciarri *et al.*, Phys. Lett. **B467** (1999) 171;
DELPHI Collaboration, P. Abreu *et al.*, Phys. Lett. **B502** (2001) 9;
ALEPH Collaboration, A. Heister *et al.*, Eur. Phys. J. **C19** (2001) 1.
- [6] L3 Collaboration, M. Acciarri *et al.*, Phys. Lett. **B403** (1997) 168;
L3 Collaboration, M. Acciarri *et al.*, Phys. Lett. **B436** (1998) 417;
ALEPH Collaboration, R. Barate *et al.*, Phys. Lett. **B462** (1999) 389;
L3 Collaboration, M. Acciarri *et al.*, Phys. Lett. **B487** (2000) 229;
L3 Collaboration, P. Achard *et al.*, Phys. Lett. **B547** (2002) 151.
- [7] ALEPH Collaboration, R. Barate *et al.*, Phys. Lett. **B445** (1998) 239.
- [8] CDF Collaboration, F. Abe *et al.*, Phys. Rev. Lett. **78** (1997) 4536;
DØ Collaboration, B. Abbott *et al.*, Phys. Rev. **D60** (1999) 072002.
- [9] Physics at LEP2, edited by G. Altarelli, T. Sjöstrand and F. Zwirner, CERN 96-01 Vol. 1, 525.
- [10] K. Hagiwara, R.D. Peccei, D. Zeppenfeld and K. Hikasa, Nucl. Phys. **B282** (1987) 253.

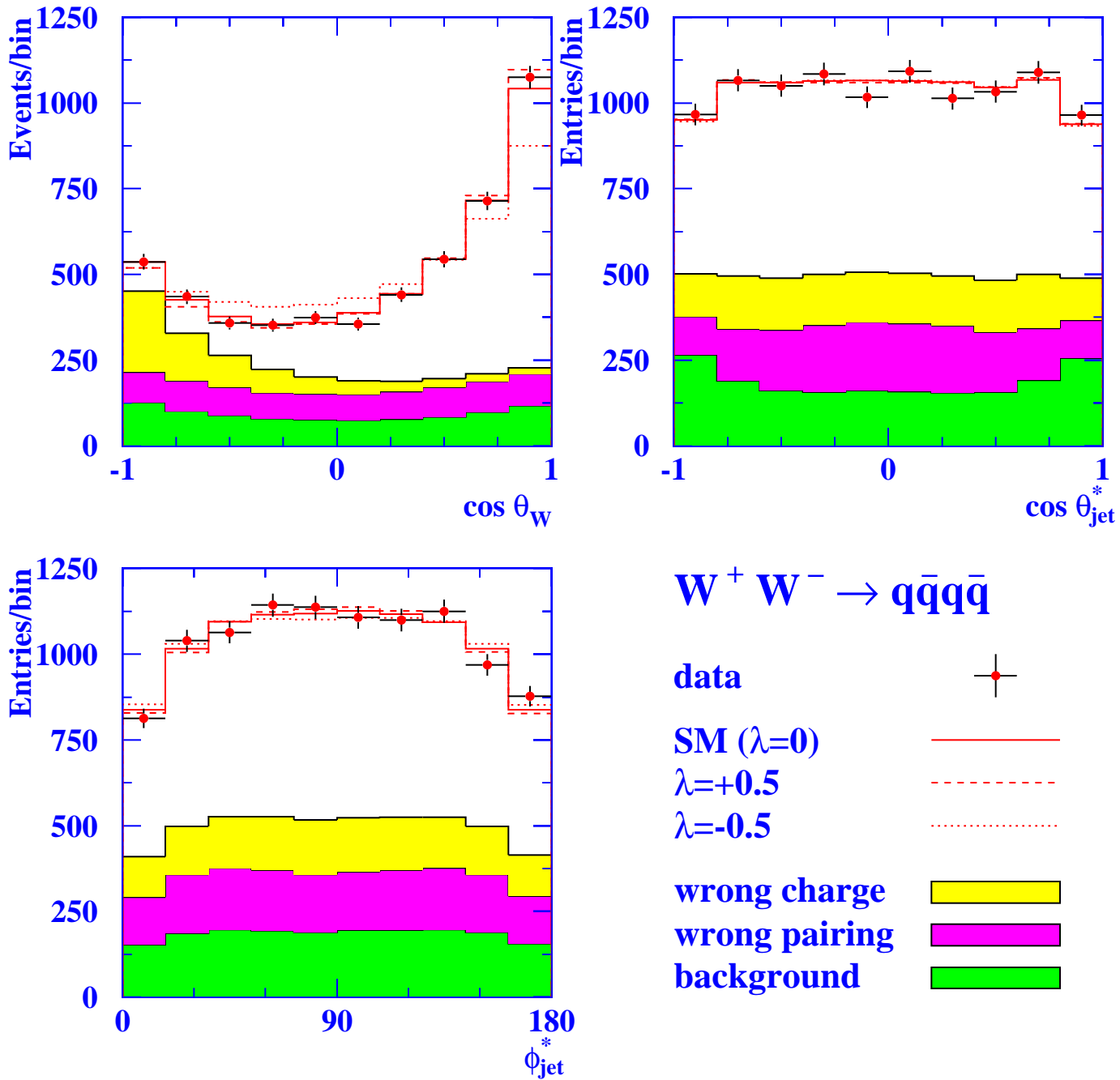
- [11] M. Bilenky, J.L. Kneur, F.M. Renard and D. Schildknecht, Nucl. Phys. **B409** (1993) 22; Nucl. Phys. **B419** (1994) 240.
- [12] K. Gaemers and G. Gounaris, Z. Phys. **C1** (1979) 259.
- [13] OPAL Collaboration, G. Abbiendi *et al.*, Eur. Phys. J. **C19** (2001) 229.
- [14] A. De Rujula, M.B. Gavela, P. Hernandez and E. Masso, Nucl. Phys. **B384** (1992) 3.
- [15] K. Hagiwara, S. Ishihara, R. Szalapski and D. Zeppenfeld, Phys. Lett. **B283** (1992) 353; Phys. Rev. **D48** (1993) 2182.
- [16] R.L. Sekulin, Phys. Lett. **B338** (1994) 369.
- [17] OPAL Collaboration, K. Ahmet *et al.*, Nucl. Instr. Meth. **A305** (1991) 275; M. Arignon *et al.*, Nucl. Instr. Meth. **A313** (1992) 103; D.G. Charlton, F. Meijers, T.J. Smith and P.S. Wells, Nucl. Instr. Meth. **A325** (1993) 129; J.T.M. Baines *et al.*, Nucl. Instr. Meth. **A325** (1993) 271; M. Arignon *et al.*, Nucl. Instr. Meth. **A333** (1993) 320; B.E. Anderson *et al.*, IEEE Transactions on Nuclear Science, **41** (1994) 845; S. Anderson *et al.*, Nucl. Instr. Meth. **A403** (1998) 326; G. Aguillion *et al.*, Nucl. Instr. Meth. **A417** (1998) 266.
- [18] S. Jadach *et al.*, Comp. Phys. Comm. **140** (2001) 475.
- [19] S. Jadach *et al.*, Phys. Rev. **D61** (2000) 113010; S. Jadach *et al.*, Comp. Phys. Comm. **140** (2001) 432.
- [20] F.A. Berends, R.Pittau and R. Kleiss, Comp. Phys. Comm. **85** (1995) 437; F.A. Berends and A.I. van Sighem, Nucl. Phys. **B454** (1995) 467.
- [21] M. Skrzypek *et al.*, Comp. Phys. Comm. **94** (1996) 216; M. Skrzypek *et al.*, Phys. Lett. **B372** (1996) 289; S. Jadach *et al.*, Comp. Phys. Comm. **119** (1999) 272.
- [22] J. Fujimoto *et al.*, Comp. Phys. Comm. **100** (1997) 128.
- [23] S. Jadach, B.F.L. Ward and Z. Was, Phys. Lett. **B449** (1999) 97; S. Jadach, B.F.L. Ward and Z. Was, Comp. Phys. Comm. **130** (2000) 260.
- [24] S. Jadach *et al.*, Comp. Phys. Comm. **79** (1994) 503.
- [25] S. Jadach, W. Placzek and B.F.L. Ward, Phys. Lett. **B390** (1997) 298.
- [26] G. Marchesini *et al.*, Comp. Phys. Comm. **67** (1992) 465.
- [27] A. Buijs *et al.*, Comp. Phys. Comm. **79** (1994) 523.
- [28] J.A.M. Vermaseren, Nucl. Phys. **B229** (1983) 347.
- [29] F.A. Berends, P.H. Daverveldt and R. Kleiss, Comp. Phys. Comm. **40** (1986) 271.
- [30] T. Sjöstrand, Comp. Phys. Comm. **82** (1994) 74.

- [31] L. Lönnblad, *Comp. Phys. Comm.* **71** (1992) 15.
- [32] OPAL Collaboration, G. Alexander *et al.*, *Z. Phys.* **C69** (1996) 543;
OPAL Collaboration, G. Abbiendi *et al.*, CERN-EP-2003-031, Submitted to *Eur. Phys. J. C*.
- [33] J. Allison *et al.*, *Nucl. Instr. Meth.* **A317** (1992) 47.
- [34] OPAL Collaboration, G. Abbiendi *et al.*, *Phys. Lett.* **B493** (2000) 249.
- [35] Tevatron Electroweak Working Group and the CDF and DØ Collaborations, “Combination of CDF and DØ Results on W Boson Mass and Width”, FERMILAB-FN-0716, August 2002.
- [36] N. Brown and W.J. Stirling, *Phys. Lett.* **B252** (1990) 657;
S. Catani *et al.*, *Phys. Lett.* **B269** (1991) 432;
S. Bethke, Z. Kunszt, D. Soper and W.J. Stirling, *Nucl. Phys.* **B370** (1992) 310;
N. Brown and W.J. Stirling, *Z. Phys.* **C53** (1992) 629.
- [37] OPAL Collaboration, K. Ackerstaff *et al.*, *Eur. Phys. J.* **C2** (1998) 213.
- [38] D. Karlen, *Computers in Physics* **12** (1998) 380,
<http://arXiv.org/abs/physics/9805018>.
- [39] G.K. Fanourakis, D. Fassouliotis and S.E. Tzamarias, *Nucl. Instr. Meth.* **A412** (1998) 465;
Nucl. Instr. Meth. **A414** (1998) 399.
- [40] M. Diehl and O. Nachtmann, *Z. Phys.* **C62** (1994) 397.
- [41] OPAL Collaboration, G. Abbiendi *et al.*, *Phys. Lett.* **B453** (1999) 153.
- [42] L. Lönnblad and T. Sjöstrand, *Eur. Phys. J.* **C2** (1998) 165.
- [43] T. Sjöstrand and V.A. Khoze, *Z. Phys.* **C62** (1994) 281; *Phys. Rev. Lett.* **72** (1994) 28.

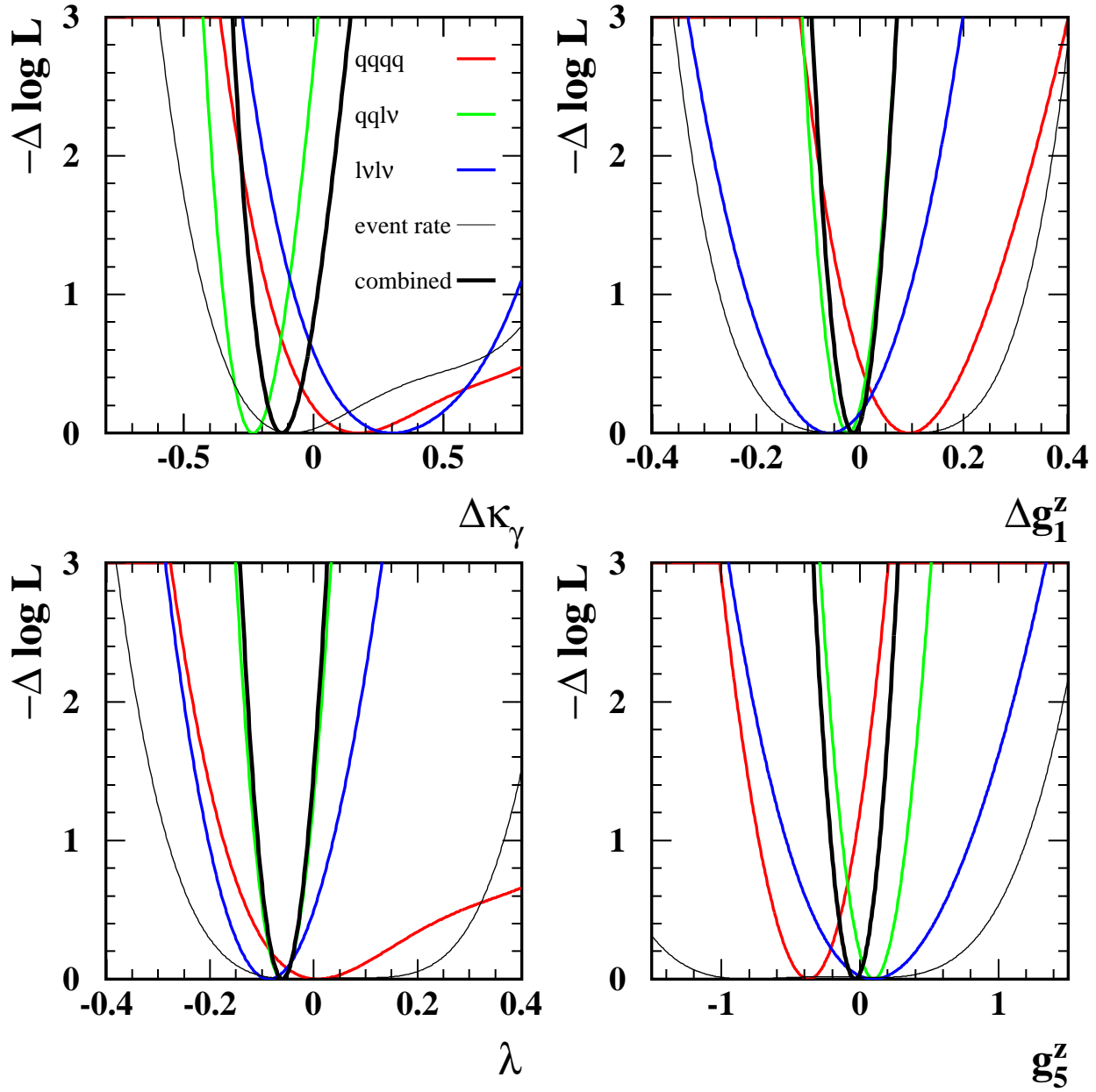
OPAL



OPAL



OPAL



OPAL

